Fuel 415 (2026) 138370

Contents lists available at ScienceDirect

Fuel

journal homepage: www.elsevier.com/locate/fuel

Full Length Article

Hybrid H_2 storage in ZIF-8 and THF-driven Hydrates: A molecular simulation study at the microsecond scale

Fengyi Mi [a], Hongjuan Sun [a,*], Wei Li [b], Bin Fang [d], Zhun Zhang [b], Bowen Sha [c], Thijs J.H. Vlugt [c], Othonas A. Moultos [c,*], Fulong Ning [b,*]

[a] Key Laboratory of Solid Waste Treatment and Resource Reuse, Ministry of Education, Southwest University of Science and Technology, Mianyang 621010, Sichuan, China
[b] National Center for International Research on Deep Earth Drilling and Resource Development, Faculty of Engineering, China University of Geosciences, Wuhan, Hubei 430074, China
[c] Engineering Thermodynamics, Process & Energy Department, Faculty of Mechanical Engineering, Delft University of Technology, Leeghwaterstraat 39, Delft 2628CB, the Netherlands
[d] School of Marine Science and Engineering, Hainan University, Haikou 570228, China

ARTICLE INFO

Keywords:
Hydrogenstorage
MOF
Molecular dynamics simulation
Binary hydrogen hydrate
Physisorption.

ABSTRACT

Hydrogen can play a central role in a fossil-free energy economy, yet its implementation is hindered by the lack of safe, dense, and efficient storage methods. Hybrid H_2 physisorption-hydrate formation, which combines physisorption in porous materials with encapsulation in clathrate hydrates, presents a promising route, but the fundamental synergistic mechanisms remain largely elusive. Here, we perform microsecond-scale molecular dynamics simulations to study the hybrid H_2 storage process in the hydrophobic metal–organic framework ZIF-8 seeded with THF hydrate nanoparticles. The results indicate that ZIF-8 rapidly physisorbs H_2, while effectively excluding H_2O and THF. Our simulations reveal a dynamic, three-step hybrid storage pathway, *i.e.*, (1) ZIF-8 selectively adsorbs and enriches H_2 within its pores, creating a high local H_2 concentration; (2) The growing binary H_2-THF hydrate crystals selectively capture the H_2; (3) Transfer of H_2 from the ZIF-8 to the hydrate until the hydrogen source transfer reaches a dynamic equilibrium. This hybrid storage method results in a total H_2 storage capacity reaching 1.82 wt%, exceeding the storage capacity of either physisorption or THF-driven hydrate formation alone. These findings provide critical molecular-level insights, showing that coupling hydrophobic ZIF-8 with hydrate promoters is a highly effective strategy for developing next-generation H_2 storage methods.

1. Introduction

Hydrogen (H_2) is an important energy carrier owing to its high energy density and zero-carbon combustion products. As decarbonization efforts accelerate globally, efficient H_2 utilization in fuel cells, power generation, and industrial processes becomes critical. However, persistent storage challenges hinder widespread use of H_2 energy technologies due to the low volumetric density (0.08 g/L) and high flammability of H_2 [1,2]. Compressed of H_2 storage requires pressures in excess of 70 MPa to achieve moderate volumetric density [3]. Liquefied of H_2 demands cooling to below 20 K, which results in significant energy demands and evaporation losses [4]. Metal hydrides offer high volumetric capacity but suffer from heavy weight, sluggish absorption/desorption kinetics, and high operating temperatures [5]. Porous materials such as metal–organic frameworks (MOFs) can moderately absorb H_2 at low temperatures; their capacity is limited at ambient conditions [6]. These disadvantages highlight the urgent need for alternative storage solutions that can simultaneously offer high volumetric density, fast kinetics, and operational safety under relatively mild conditions. Clathrate hydrates are sustainable nanomaterials formed by the oriented arrangement of water molecules [7,8]. The volume storage density of H_2 hydrate can reach or exceed that of liquid H_2 storage under moderate pressure and low temperature conditions [9–11]. However, its practical application is often hindered by slow formation kinetics and demanding operational conditions, challenges that primarily stem from the low solubility of H_2 in the aqueous phase. H_2 storage of hybrid physisorption-hydrate

* Corresponding authors.
E-mail addresses: sunhongjuan@swust.edu.cn (H. Sun), o.moultos@tudelft.nl (O.A. Moultos), nflzx@cug.edu.cn (F. Ning).

https://doi.org/10.1016/j.fuel.2026.138370
Received 30 October 2025; Received in revised form 1 January 2026; Accepted 11 January 2026
Available online 19 January 2026

formation has attracted great attention, since it combines rapid physisorption with hydrate formation to exploit the advantages of both mechanisms, and mitigate their individual drawbacks.

Early studies focused on the formation of pure H_2 hydrates, which require extremely high pressures (200 MPa). To overcome these extreme conditions, effort was put to the study of binary hydrates, where promoter molecules can greatly reduce the formation pressure of H_2 hydrates [12–15]. Methane, carbon dioxide, propane, cyclopentane, and tetrahydrofuran (THF) are all common promoters of H_2 hydrate formation [16–20]. In a previous study, we performed molecular dynamics (MD) simulations to investigate the formation of binary H_2 hydrates for different promoters [21]. The simulation results showed that THF was the most efficient promoter for binary H_2 hydrate formation [21]. The experimental results of Lee *et al.* showed that THF molecules occupied large cavities to stabilize the binary H_2 hydrate structure, thereby reducing the pressure conditions for H_2 storage from 200 MPa to 12 MPa [11]. Many experimental and MD studies have investigated the effects of promoter concentration [22,23], temperature [24], pressure [24,25], and driving force [26–28] on the formation of binary H_2 hydrates. Monte Carlo (MC) simulations [29] have examined the storage capacity of the mixed H_2 + THF hydrate under different thermodynamic conditions. An extensive discussion addressing the comparison of experimental and MC studies for the H_2 storage capacity of the particular mixed hydrate has been presented in [30]. MC studies for calculating H_2 storage capacity of different hydrate structures and promoters has been reviewed in [31]. Moreover, porous materials can greatly enhance the formation kinetics of gas hydrates due to their large amount of confined space and surface area [32,33]. Farrando-Perez and co-workers designed new porous activated carbon materials that greatly improve the kinetics of H_2 hydrate formation [34]. Ciocarlan *et al.* designed hydrophobic mesoporous silica as the host material, which significantly reduced the pressure required to form H_2 hydrate (about 20 %) [35]. MOFs have been extensively investigated for gas storage due to their high surface areas and tunable pore environments [36,37]. Previous experiments and simulation studies have shown that MOFs were used to store methane gas via a hybrid physisorption-hydrate formation method, which improved the gas storage capacity [38–40]. Hydrophobic MOFs such as ZIF-8 not only physisorb small gas molecules but also promote heterogeneous hydrate nucleation at interfaces [41–43]. Most studies have treated physisorption [44] and hydrate formation [8] separately for H_2 storage in hydrophobic ZIF-8, without investigating coupled mechanisms affecting H_2 storage (especially the synergistic effect of THF promoters remains unclear).

Here, we perform microsecond-scale MD simulations to investigate hybrid H_2 physisorption-hydrate formation in hydrophobic ZIF-8 seeded with THF hydrate nanocrystals. Our results show a three-step hybrid H_2 storage pathway, *i.e.*, rapid enrichment, targeted capture, and dynamic transfer of H_2. The total H_2 storage capacity (physisorption and hydrate storage) far exceeds that achievable by a single mechanism, reaching 1.82 wt% and is predicted to even exceeding 5 wt% after a long time. These findings indicate that coupling hydrophobic ZIF-8 with hydrate promoters is a highly effective strategy for developing next-generation H_2 storage methods.

2. Simulation details and methods

The initial configuration comprised 1 ZIF-8, 1 THF hydrate nanoparticle, 6000 H_2, 550 THF, and 15,195 H_2O molecules·THF is most favourable for binary H_2 hydrate nucleation as shown in the literature [21]. We replicated the cell of ZIF-8 to create a ZIF-8 structure with dimensions 2 × 2 × 2, which was then placed in the simulation box. A nanoparticle of THF hydrate (structure II) was inserted into the simulation box before solvation. Water molecules were then added to fully hydrate the system. The final composition (see Fig. 1) reflects a mixture of ZIF-8, H_2, and water, with THF hydrate crystals acting as seeds for hydrate growth·THF hydrate nanoparticles contain 33 THF molecules

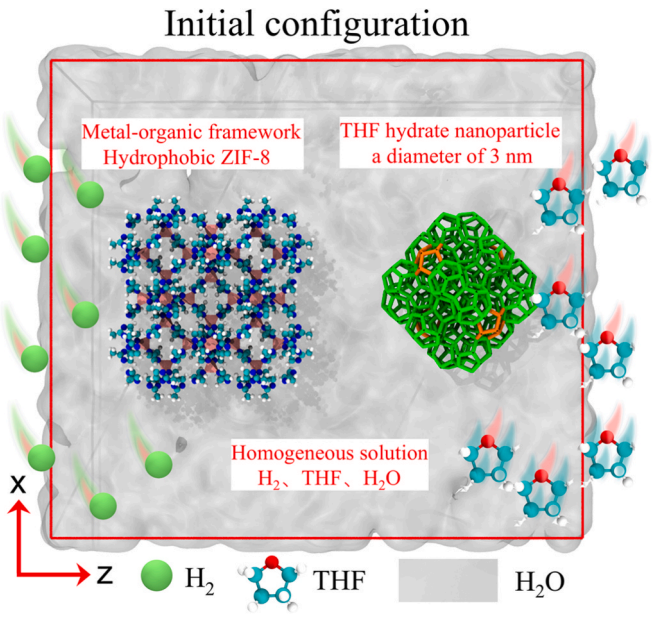

Fig. 1. Schematic representation of the initial configuration of the MD simulation. The hydrophobic metal–organic framework ZIF-8, hydrate nanoparticle, and H_2O solution are shown. The initial homogeneous solution is composed of H_2, THF, and H_2O molecules.

and 481 H_2O molecules, which is consistent with the ratio of large cages to H_2O molecules in the SII-type hydrate [45]. Five independent simulations, each one starting from a different initial configuration, were performed to obtain statistics. Specifically, different random seeds were used for the free molecules (H_2, THF, and H_2O), ensuring statistically independent trajectories. In total, five independent simulations of H_2 storage in MOF ZIF-8 were tested and marked as H_{MOF1}, H_{MOF2}, H_{MOF3}, H_{MOF4}, and H_{MOF5}. Details on the composition of these systems are listed in Table S1. Periodic boundary conditions were applied in all directions.

The force field parameters for the MOF ZIF-8 were taken from Zheng *et al.* [46,47]. THF and H_2O molecules were modeled using the OPLS-AA [48] and TIP4P/Ice force fields [49], respectively, which have achieved high accuracy in previous MD studies [50–52]. For H_2, the three-site model developed by Alavi *et al.* [53] was used. All force field details are listed in Table S2 in the Supporting Information. These force fields were shown in previous MD studies to perform well in modelling the nucleation process of clathrate hydrates [24,25,27,54–58]. To maintain the stability of ZIF-8, ZIF-8 was treated as a rigid structure. The Lorentz-Berthelot mixing rules were used for the cross interactions. The leapfrog integration algorithm was used in the MD simulation with a 2.0 fs timestep. As shown in Fig. S1, the total energy fluctuates around a stable mean value with no significant drift over the simulation period, confirming that the 2 fs time step does not compromise the numerical stability of the system [59]. Production runs of 2 μs were performed under the isothermal-isobaric (*NPT*) ensemble at a pressure of 50 MPa and a temperature of 250 K. These conditions fall well within the experimental stability region of THF hydrates [25]. These conditions ensure that the time required for hydrate nucleation is accessible in the molecular simulation, and thus, within reasonable computational costs [60–62]. To regulate the temperature and pressure, the Nosé-Hoover thermostat [63] and Parrinello-Rahman barostat [64] with time constants of 2 ps and 4 ps, respectively, were used. MD simulations were performed in GROMACS 2022 [65]. All simulation details (*e.g.*, initial configurations, equilibration scheme, electrostatics) along with the calculation principles of the properties computed in this study are provided in the Supporting Information.

3. Results and Discussions

3.1. Distribution of guest molecules, and metal–organic framework ZIF-8-guest molecule interactions

The distribution of guest molecules and their interaction with ZIF-8 affect the physisorption of H_2 in ZIF-8 and the growth of binary H_2-THF hydrate in the aqueous phase. The radial distribution functions (RDF) of the metal–organic framework ZIF-8 with H_2 and H_2O molecules are shown in Fig. 2a-b and Figs. S2-S3 in the supporting information. The RDF for H_2 molecules shows that the structure of H_2 molecules and ZIF-8 atoms is consistent with the pore size range (Fig. 2a and Fig. S2a-e). Specifically, a peak at approximately 0.3–0.5 nm for the C-H_2 shows that H_2 is close to the organic ligands (Fig. 2a and Fig. S2a-e); The Zn-H_2 peak occurs over longer distances, indicating that H_2 is adsorbed close to the metal nodes Zn (Fig. 2a and Fig. S2a-e). These broad peaks of Zn-H_2 indicate that H_2 is physically adsorbed in the ZIF-8 pores. In contrast, the weak peak of the RDF curve corresponding to H_2O reflects the hydrophobic nature of the ZIF-8 (Fig. 2b and Fig. S3a-e), *i.e.*, H_2O molecules entering ZIF pores are unfavourable. These results confirm that ZIF-8 selectively adsorbs H_2 molecules, while repelling H_2O molecules due to steric interactions, thereby forming a distinct interface between the gaseous H_2 and aqueous THF phases (Figs. S4-S7). The number density profiles in Fig. 2c and Figs. S4-S7 show the spatial distribution of guest molecules in the system. Due to the geometry of the H_2 nanobubble, the projection of density onto the z-axis results in an apparent spatial overlap between the gas phase and the ZIF-8 surface region (0–4 nm). We find that the high density of H_2 in the 0–4 nm region corresponds to the nanobubble, while the specific peaks within the ZIF-8 framework correspond to adsorbed molecules. Moreover, visual inspection of the simulation trajectories (as shown in Fig. 2c) confirms that mainly H_2 is contained within the nanobubbles. As can be observed in Fig. 2c and Figs. S4-S5, H2 has a relatively high density both inside the ZIF-8 pores and in the bubble region, while H_2O is mainly concentrated outside the ZIF-8 (Fig. 2c and Fig. S6a-e), indicating that liquid water is excluded from the hydrophobic ZIF-8 pores. The density distribution of THF molecules is similar to that of H_2O, and it does not reside in the ZIF-8 pores (Figs. S6-S7). This means that ZIF-8 can selectively capture H_2 molecules while excluding H_2O and THF, forming an interface where the gas phase (H_2 in the pores) and the H_2O phase (H_2O/THF outside the pores) coexist, creating favorable conditions for the heterogeneous hydrate nucleation. As can be observed in Fig. 2c and Figs. S5, H2 aggregates into nanobubbles within the aqueous phase. It should be noted that these H_2 nanobubbles exhibit an internal pressure higher than the system's nominal bulk pressure (50 MPa) due to the surface tension effect described by the Young-Laplace equation. In experimental hydrogenation or gas storage processes, involving dispersed gas phases, such as micro- or nanobubbles, is a common approach [23,43,66].

The diffusion and residence of H_2 in different phases are illustrated in Fig. 2d-f. Simulation snapshots reveal that H_2 has four states, namely H_2 (1) in hydrates, (2) in water, (3) in ZIF-8, and (4) in nanobubbles (Fig. 2e). As can be seen in the Fig. 2e, water molecules are effectively rejected from the internal pore structure of the ZIF-8 framework, interacting only with the external surface. The diffusion coefficients of these states all change rapidly at the beginning of the simulation and then enter a plateau (Fig. 2d and Fig. S8a-e). The diffusion coefficient of H_2 in nanobubbles is the highest; the diffusion coefficient of H_2 in the aqueous phase is moderate (Fig. 2d and Fig. S8a-e). As expected, H_2 adsorbed onto the ZIF-8 pores diffuses the slowest due to the nanoconfinement effect. The change in the diffusion coefficient in the early stage of the simulation is attributed to the phase separation of H_2 molecules, some of which rapidly diffuse into the ZIF-8 pores. The diffusion coefficient of H_2 in the aqueous phase gradually decreases, attributed to the fact that some H_2 molecules in the aqueous phase are bound to hydrate cages (Fig. 2d-e), significantly restricting their movement. The probability distribution of the residence time for H_2 in ZIF-8 shows that most H_2 adsorbed in ZIF-8 pores resides for only tens of picoseconds (Fig. 2f and Fig. S9a-e), indicating rapid adsorption–desorption exchange with the external environment. The residence time of the H_{MOF2} system is highest (Fig. 2f and Fig. S9a-e), likely due to the absence of

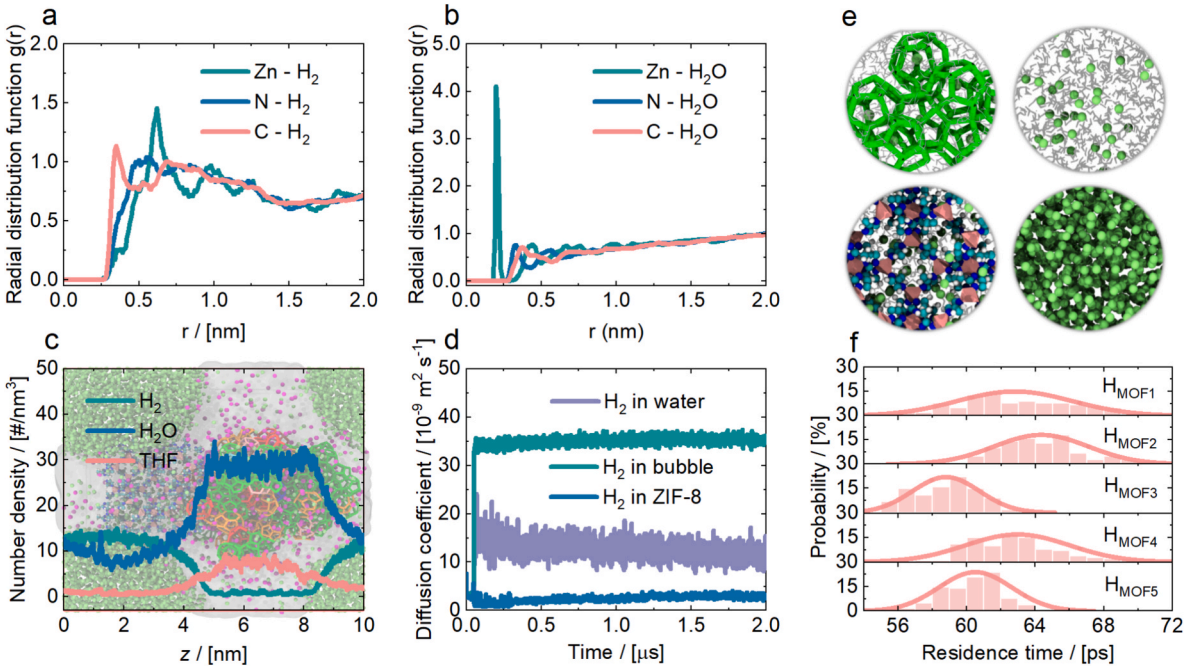

Fig. 2. Radial distribution functions $g(r)$ ZIF-8 atoms (*i.e.*, Zn, N, and C) with (a) H_2 and (b) H_2O molecules. (c) Number density distribution of H_2, H_2O, and THF molecules in the z direction for the H_{MOF1} system. (d) Time evolution of the average diffusion coefficient for H_2 in water, bubble, and ZIF-8. (e) Snapshots of H_2 in hydrate, water, ZIF-8, and bubble. (f) Probability distribution of the residence time for H_2 in ZIF-8. Lime balls and silver lines represent H_2 and H_2O molecules, respectively. Bonds of green colours represent 5^{12} hydrate cages. (For interpretation of the references to colour in this figure legend, the reader is referred to the web version of this article.)

hydrates. Hydrates compete with ZIF-8 for H_2 molecules in the H_{MOF1}, H_{MOF3}, H_{MOF4}, and H_{MOF5} systems, thereby reducing the residence time of H_2 molecules in ZIF-8 pores. These results indicate that the hydrophobic ZIF-8 pores selectively adsorb H_2 (physisorption) while simultaneously repel liquid water, forming a gas–water interface on the pore surface. This increased gas–water interface facilitates the heterogeneous nucleation of hydrates.

3.2. Physisorption of H_2/THF on ZIF-8

During the physisorption process, the distribution of H_2/THF molecules in the ZIF-8 pores at 2 μs is shown in Fig. 3a-b. A large number of H_2 molecules occupy the ZIF-8 pore space, while only a very small number of THF molecules enter the ZIF-8 pores (Fig. 3a-b), favoring the storage of H_2 in the ZIF-8 pores via physisorption. To further monitor the adsorption process of H_2/THF in the ZIF-8 pores, the evolution of the number of adsorbed H_2/THF molecules in the ZIF-8 pores for five different systems is shown in Fig. 3c-d and Fig. S10a-e. The number of H_2 molecules in the ZIF-8 pores in each system rapidly increases (Fig. 3c-d and Fig. S10a-e), indicating that the adsorption sites are filled within a short time. Subsequently, the number of H_2 molecules in the ZIF-8 pores gradually decreases within the simulation period of 0.2–1.0 μs (Fig. 3c-d and Fig. S10a-e). This is attributed to the fact that the growth of binary H_2-THF hydrate requires a hydrogen source, resulting in the gradual migration of H_2 molecules within the ZIF-8 pores to the exterior of the pores for binary H_2-THF hydrate growth. Competition for hydrogen sources between the growth of binary H_2-THF hydrate and the physisorption of H_2 in ZIF-8 results in a trade-off. This results in a plateau in the number of H_2 molecules in the ZIF-8 pores during a simulation period of 1.0–2.0 μs (Fig. 3c-d and Fig. S10a-e). The H_{MOF2} system exhibits the lowest H_2 adsorption, consistent with its inability to form binary H_2-THF hydrates. In contrast, less than 0.8 % of THF molecules are present in ZIF-8, and the THF adsorption in each system is significantly lower than that of H_2 (Fig. 3c-d and Fig. S10a-e). In particular, THF in ZIF-8 systems primarily accumulates near the ZIF-8 surface rather than within the ZIF-8 pores (Fig. 3b). This is primarily due to the larger size of THF molecules, and their weak interaction with ZIF-8.

To study the adsorption strength of H_2/THF molecules in the ZIF-8 pores, the lifetimes of H_2/THF molecules in ZIF-8 pores are computed (Fig. 3e-f). The stronger the adsorption strength of H_2/THF in ZIF-8 pores is, the longer its lifetime in ZIF-8 pores will be. The lifetime of H_2/THF molecules in ZIF-8 pores is defined as the time during which the H_2/THF molecule retains its state in ZIF-8 in subsequent simulations divided by the total subsequent time. H_2 molecules in the ZIF-8 pores exhibit a short residence time, with a lifetime of approximately 2–3 % (Fig. 2f and Fig. 3e), indicating their rapid adsorption–desorption. In contrast, THF molecules exhibit a long residence time, with a lifetime extending 20 % (Fig. 3f and Fig. S9a-e), indicating that once THF is adsorbed near ZIF-8, it remains in the adsorption state for a long time. Notably, the lifetime of H_2 molecules in the ZIF-8 pores in the H_{MOF2} system can reach as high as 9 %, significantly exceeding these lifetimes in the other four systems, *i.e.*, H_{MOF1}, H_{MOF3}, H_{MOF4}, and H_{MOF5} systems (Fig. 3e). This suggests that the growth of binary H_2-THF hydrates in the external space of ZIF-8 pores weakens the adsorption strength of H_2 in the ZIF-8 pores, which is unfavorable for the storage of H_2 via physisorption. An interesting future research route could focus on reducing this adverse effect, such as designing new MOF materials with stronger H_2 binding capabilities or increasing the hydrogen source in the aqueous phase. Taken together, these results indicate that ZIF-8 pores can efficiently and temporarily store H_2 molecules, and once THF is near ZIF-8, it exhibits more stable adsorption characteristics.

3.3. Growth kinetics of binary H_2-THF hydrates in ZIF-8

The growth process of binary H_2-THF hydrates in different systems is

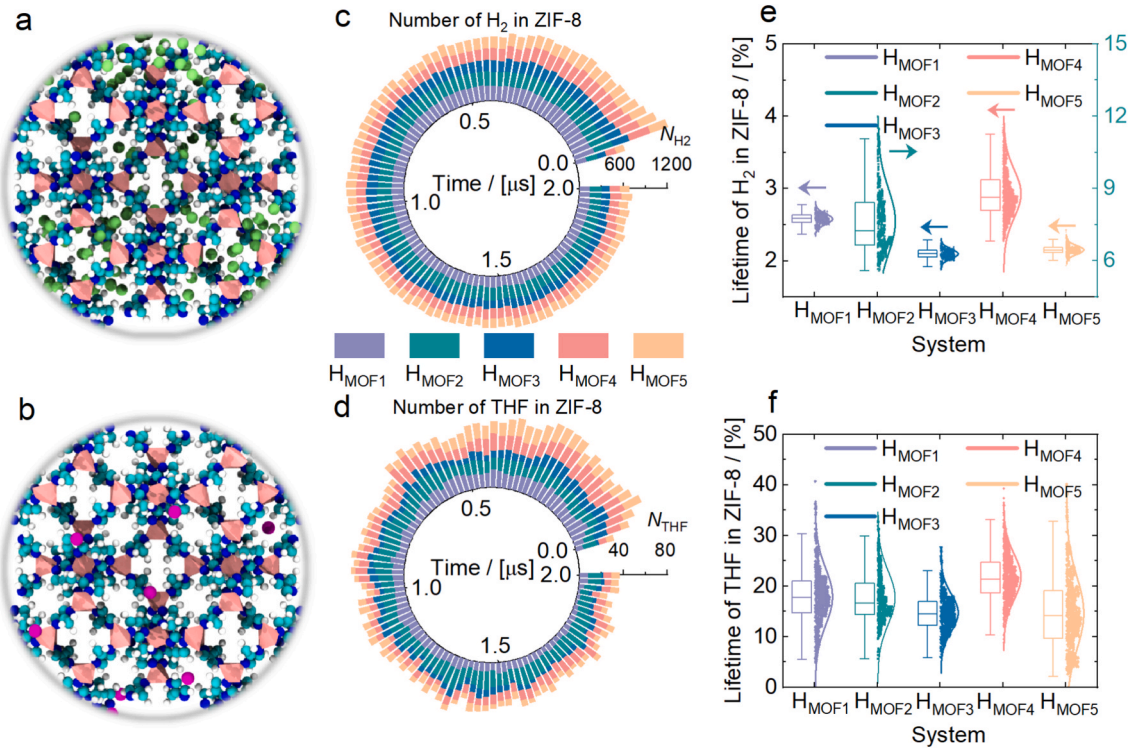

Fig. 3. Simulation snapshots of (a) H_2 and (b) THF in ZIF-8 pores. Evolution of the number of (c) H_2 and (d) THF in ZIF-8 pores for the five systems. Lifetimes of (e) H_2 and (f) THF in ZIF-8 pores for the five systems, *i.e.*, H_{MOF1}, H_{MOF2}, H_{MOF3}, H_{MOF4}, and H_{MOF5}. Hydrophobic metal–organic framework ZIF-8 is displayed as pink (Zn atom), cyan (C atom), blue (N atom), and white (H atom). Magenta balls and lime balls represent THF and H_2 molecules, respectively. (For interpretation of the references to colour in this figure legend, the reader is referred to the web version of this article.)

displayed in Fig. 4a-e and Videos S1-S5. For a detailed description of the phase evolution in each system, including the dissociation process observed in H_{MOF2}, figures showing the time-evolution are provided in the Supporting Information (Figs. S11-S15 and Videos S1-S5). In the H_{MOF1} system, initial hydrate nanoparticles gradually grow, forming large hydrate crystals close to the ZIF-8 at a simulation time of 2 μs (Fig. 4a and Fig. S11). Gradual hydrate crystal growth is also observed in H_{MOF3}, H_{MOF4}, and H_{MOF5} systems (Fig. 4c-e and Figs. S12-S14), although the timing of onset and the final number of hydrates vary. Notably, the snapshots of the H_{MOF2} system show almost no hydrate crystal at 2 μs (Fig. 4b and Fig. S15). Initially, the hydrate nanoparticles in the H_{MOF2} system gradually decompose, and no large hydrate crystals remain for a long time during the rest of the simulation (Fig. 4b and Fig. S12). Therefore, among the five simulation systems, only the H_{MOF2} system fails to form binary H_2-THF hydrates; the remaining four systems all enter the hydrate growth stage (Videos S1-S5).

To study the growth kinetics of binary H_2-THF hydrates, the evolution of the F_4 order parameter, number of hydrate cages, guest molecule mole fraction, and number of guest molecules in the nanobubble are calculated, and the results are shown in Fig. 5a-e. The F_4 parameters are commonly used to characterize the phases of water molecules, with the F_4 values for the liquid phase, ice phase, and hydrate phase being −0.04, −0.4, and 0.7, respectively, as stated in [67]. All systems exhibit very low F_4 values at the beginning of the simulation (Fig. 5a). For systems where hydrates grow (H_{MOF1}, H_{MOF3}, H_{MOF4}, and H_{MOF5}), the F_4 values rise rapidly, reaching approximately a value of 0.125 at a simulation time of 2 μs, indicating a gradual transition from disordered to ordered cage structures (Fig. 4a-e and Fig. 5a). Correspondingly, the number of binary H_2-THF hydrate cage in these systems increases from 0 to hundreds (Fig. 5b and Fig. S16a-e). The F_4 value for the H_{MOF2} system remains consistently ca. 0, and the number of hydrate cages remains 0, fully demonstrating the absence of hydrate crystals in the H_{MOF2} system (Fig. 4b, 5a-b, and Fig. S16a-e). The F_4 value distribution at different distances from the ZIF-8 surface is shown in Fig. 5c and Fig. S17a-e. In all hydrate growth systems, the F_4 values of water molecules close to the ZIF-8 surface are significantly lower than those farther away (Fig. 5c and Fig. S17a-e), indicating that hydrate crystals are primarily concentrated in the outer region away from the ZIF-8. This is attributed to the gradual growth of hydrate nanoparticle seeds toward the ZIF-8.

In the H_{MOF1}, H_{MOF3}, H_{MOF4}, and H_{MOF5} systems, the mole fraction of H_2 molecules in water increases, while the mole fraction of THF molecules in water decreases (Fig. 5d). This phenomenon arises from the reorganization of water molecules into cage-like structures, resulting in more H_2 being bound to hydrate cages. H_2 nanobubbles provide a direct hydrogen source for hydrate growth. Hydrate growth continuously reduces the number of H_2 molecules in the nanobubbles and increases the H_2 mole fraction in water (Fig. 5d-e and Fig. S18a). The increase in the number of THF molecules in the nanobubbles results in a decrease in the THF mole fraction in water (Fig. 5d-e and Fig. S18b). In contrast, the mole fraction of H_{MOF2} remains virtually unchanged. The number of H_2 and THF in the nanobubbles is also largely unchanged (Fig. 5d-e). The H_{MOF2} system is in a state of dynamic equilibrium, unable to drive

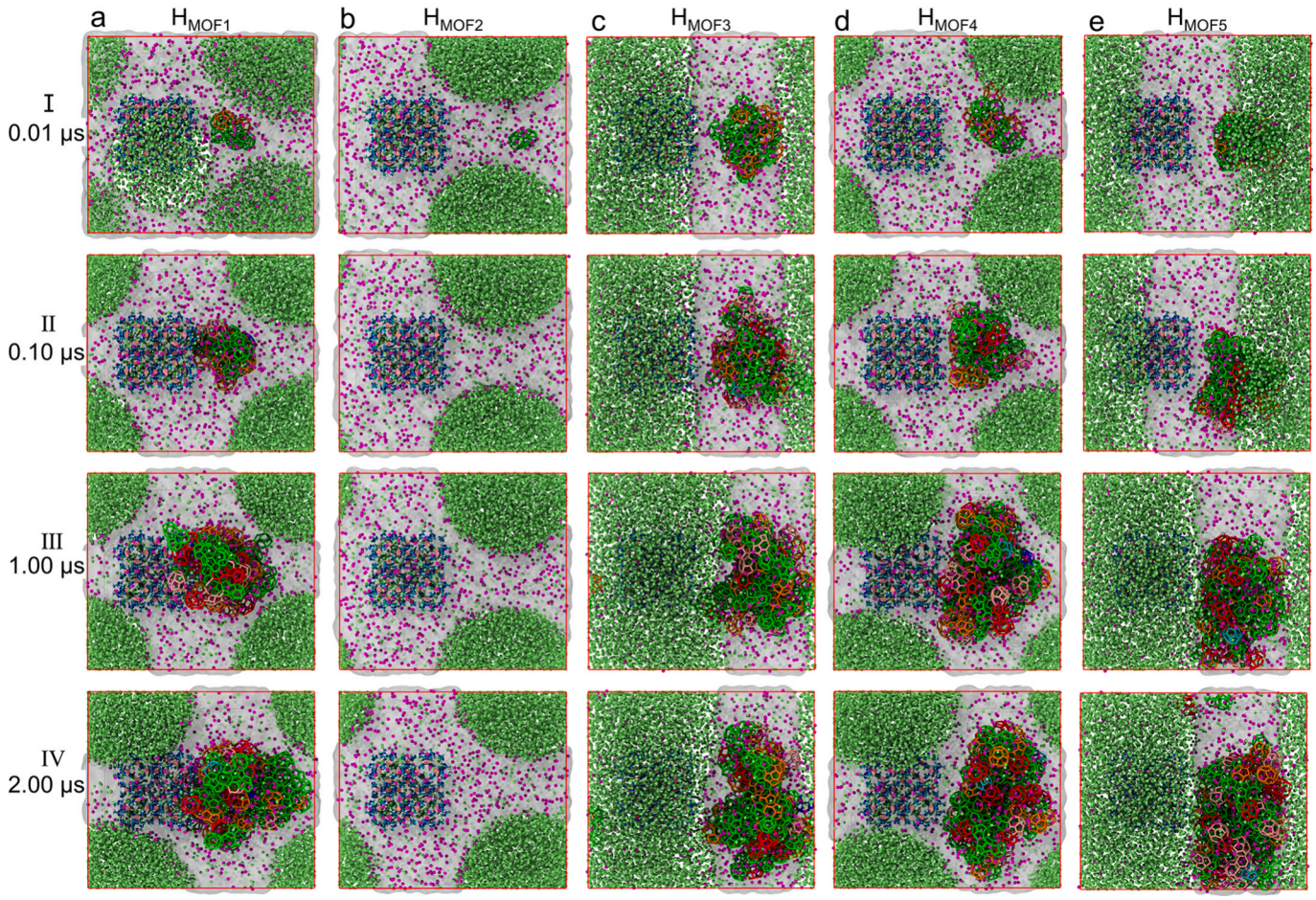

Fig. 4. Simulation snapshots showing the growth process of binary H_2-THF hydrates for the (a) H_{MOF1}, (b) H_{MOF2}, (c) H_{MOF3}, (d) H_{MOF4}, and (e) H_{MOF5} systems at 0.01, 0.10, 1.0, and 2 μ s, respectively. Hydrophobic metal–organic framework ZIF-8 is displayed as pink (Zn atom), cyan (C atom), blue (N atom), and white (H atom). Magenta balls, lime balls, and transparent white represent THF, H_2, and H_2O molecules, respectively. Bonds of different colours represent seven types of hydrate cages, *i.e.*, green for 5^{12}, blue for $5^{12}6^2$, red for $5^{12}6^3$, orange for $5^{12}6^4$, cyan for $4^15^{10}6^2$, purple for $4^15^{10}6^3$, and pink for $4^15^{10}6^4$. (For interpretation of the references to colour in this figure legend, the reader is referred to the web version of this article.)

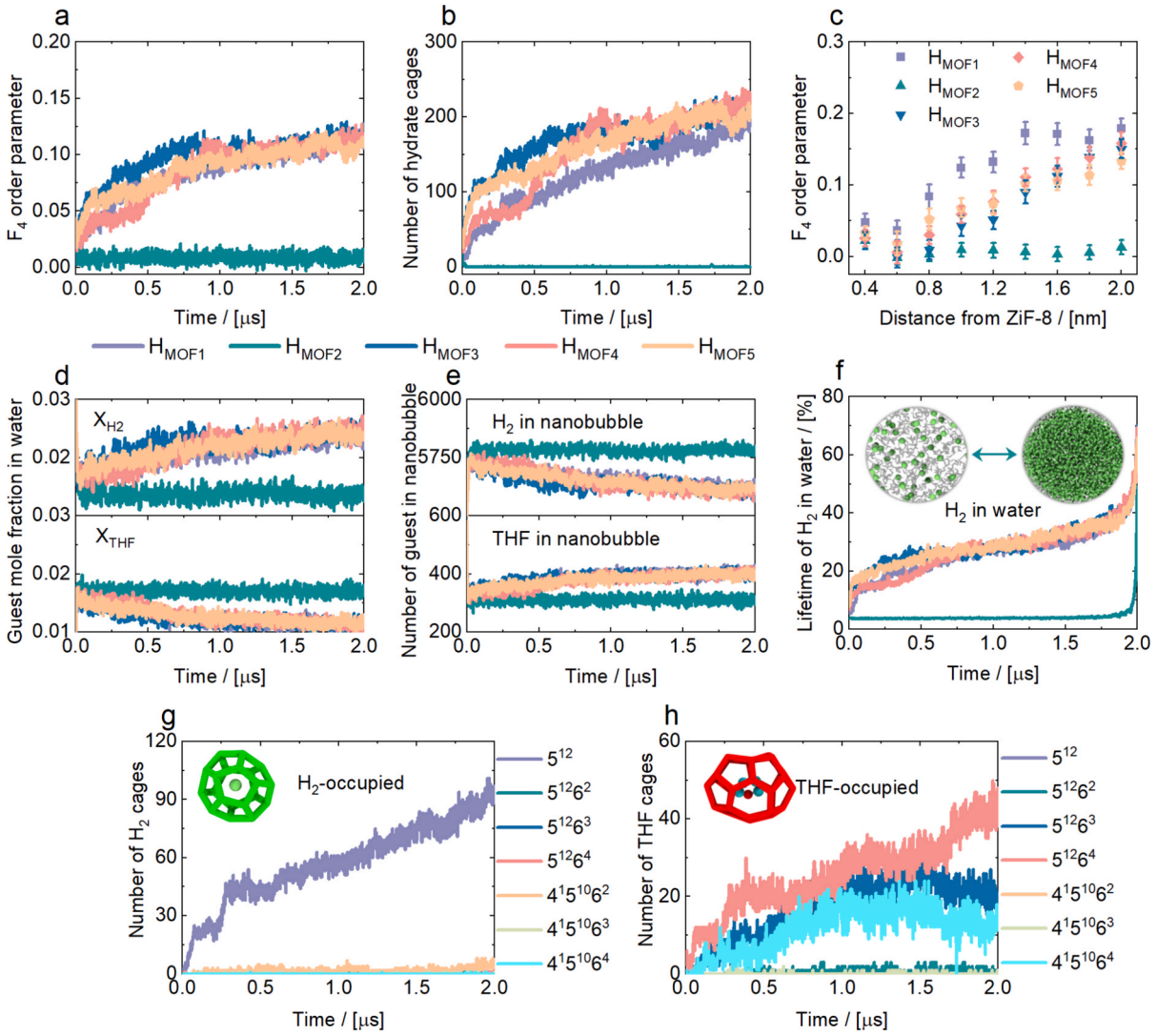

Fig. 5. Time evolution of (a) the F_4 order parameters and (b) the number of hydrate cages for five systems. (c) F_4 order parameters of the different distances from ZIF-8 averaged over the last 0.05 μs of the simulation. Time evolution of (d) the guest mole fraction in water, (e) the number of guest molecules in the nanobubble, and (f) the lifetime of H_2 molecules in water for five systems. Time evolution of the number of (g) H_2-occupied cages and (h) THF-occupied cages for the H_{MOF1} system.

hydrate nucleation and growth, further confirming the absence of hydrate crystals (Fig. 5d-e). The time evolution of the average lifetime of H_2 in water are analysed in Fig. 5f. In the H_{MOF1}, H_{MOF3}, H_{MOF4}, and H_{MOF5} systems, the lifetime of H_2 in water continuously increases, reaching 60 % in the later stages (Fig. 5f). This shows that as the hydrate crystal gradually grows, a more stable coordination environment is formed between H_2 and the surrounding H_2O, thereby extending its lifetime in water until it is finally captured in the hydrate cage. However, the lifetime of H_2 in water in the H_{MOF2} system is always short, and the lifetime value does not increase significantly with the increase of time (Fig. 5f), indicating that the structure of the water is in a highly disordered state. Moreover, H_2 mainly occupies small cages (5^{12}), while THF mainly occupies large cages ($5^{12}6^3$, $5^{12}6^4$, $4^15^{10}6^4$) (Fig. 5g-h and Figs. S19a-e, S20a-e), which is consistent with previous MD simulation results [21]. The number of guest molecules adsorbed around each H_2– and THF-occupied hydrate cage is also similar to previous MD studies (Figs. S21a-d and S22a-d) [21]. These findings regarding the order parameter, mole fraction, bubble state, and lifetime reveal that binary H_2-THF hydrates favor large cage stability, driving the rapid growth of binary H_2-THF hydrates and efficient H_2 capture via the hydrate method. Besides thermodynamic stability, the kinetics of gas release is a crucial factor for practical applications. As summarized by Alavi and Ripmeester [68], H_2 diffusion out of the hydrate phase relies on the passage of molecules through the hexagonal and pentagonal faces of the water cages. This cage-hopping mechanism is inherently slow, and it may pose a significant barrier to mass transport.

3.4. *H_2 storage mechanism via hybrid physisorption-hydrate formation in metal–organic framework ZIF-8*

A hybrid physisorption-hydrate formation significantly enhances H_2 storage capacity. Simulation snapshots of ZIF-8 physisorption and hydrate growth at different times are shown in Fig. 6 and Figs. S23-S27. For the H_{MOF1} system, H_2 molecules (green balls) are scattered around the ZIF-8 at the beginning of the simulation (0 μs), and the hydrate nanoparticle seeds are relatively distant from the ZIF-8 (Fig. 6a). During the simulation time of 0–0.01 μs, the hydrate nanoparticles become small (Fig. 6a-b), due to the interactions between the initial hydrate nanoparticles and the solution, leading to the rearrangement of the hydrate nanoparticles; A large number of H_2 molecules are observed to rapidly being adsorbed onto the ZIF-8 pores (Fig. 6a-b). During the simulation period of 0.05–0.5 μ s, a large number of H_2 molecules remain physically adsorb in the ZIF-8 pores, and some H_2 molecules diffuse from the ZIF-8 pores to the external region to form binary H_2-THF hydrates (Fig. 6c-f);

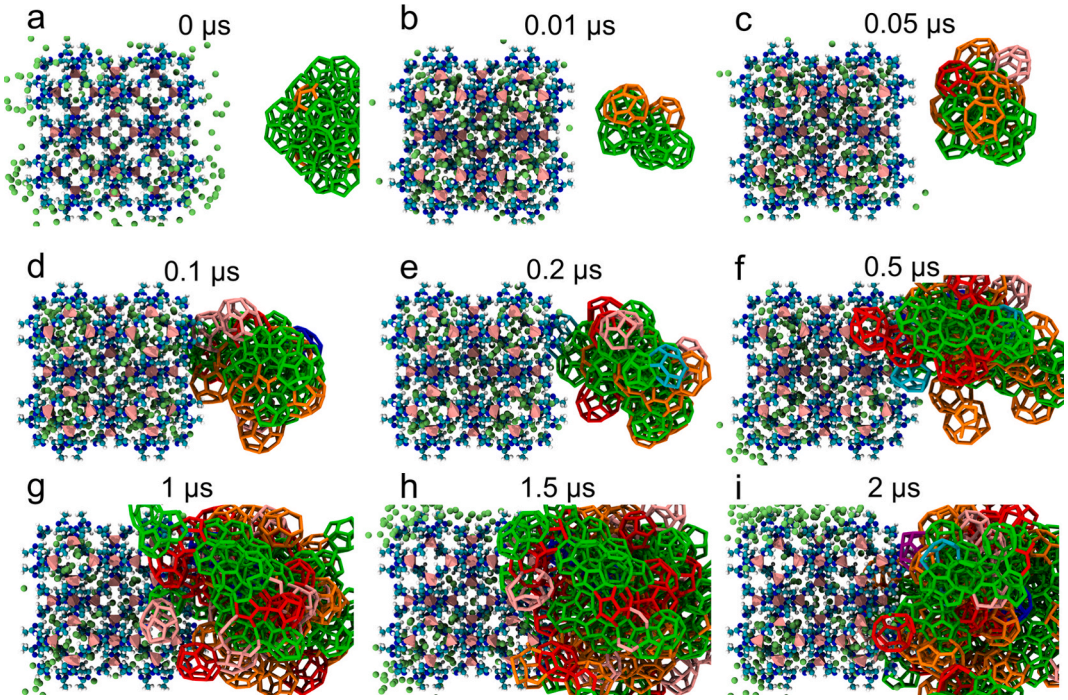

Fig. 6. Simulation snapshots showing the physisorption and hydrate growth process for the H_{MOF1} system at simulation times of (a) 0, (b) 0.01, (c) 0.05, (d) 0.1, (e) 0.2, (f) 0.5, (g) 1.0, (h) 1.5, and (i) 2 μ s. ZIF-8 is displayed as pink (Zn atom), cyan (C atom), blue (N atom), and white (H atom). Lime-coloured balls represent H_2 molecules. Bonds of different colours represent seven types of hydrate cages, *i.e.*, green for 5^{12}, blue for $5^{12}6^2$, red for $5^{12}6^3$, orange for $5^{12}6^4$, cyan for $4^15^{10}6^2$, purple for $4^15^{10}6^3$, and pink for $4^15^{10}6^4$. (For interpretation of the references to colour in this figure legend, the reader is referred to the web version of this article.)

Binary H_2-THF hydrate crystals continue to grow toward ZIF-8 (Fig. 6c-f). Over simulation periods of 0.5–2.0 μs, a large, complete hydrate crystal forms (Fig. 6g-i), which spans multiple surfaces, allowing H_2 molecules to reside both in the hydrate cages and the ZIF-8 pores (Fig. 6g-i and Figs. S23-S27).

To quantify the proportion of H_2 molecules in binary H_2-THF hydrates, the probability distribution of the H_2 ratio in the binary H_2-THF hydrates (number of cages occupied by H_2/total number of cages) is calculated and shown in Fig. 7a. The peak of the probability distribution falls in the range of 0.5–0.6 (Fig. 7a), indicating that more than half of the cage structures contain H_2. This is consistent with the characteristic that THF molecules mainly occupy a few large cages while H_2 molecules occupy many small cages (Fig. 5g-h). It is worth noting that the number of multi-occupied cages (multiple H_2 occupying the same cage) is relatively small (Fig. S27a-e). In our simulations, multi-occupancy was found to be rare, with fewer than 5 % of H_2-containing cages being occupied by more than one guest molecule. Moreover, Fig. S28a reveals the persistence of empty cages across all systems, indicating that the potential storage capacity of the hydrate lattice is not fully utilized. These situations of the small number of multi-occupied cages and the large number of empty cages will both reduce the H_2 storage capacity via the hydrate-based method. An interesting future research direction would be to focus on how to increase the number of multi-occupied cages or increase the occupancy rate of H_2 in empty cages, such as enhancing H_2 mass transfer, adding suitable hydrate particle seeds.

Understanding the mechanism of hybrid H_2 storage is crucial for developing hybrid H_2 storage methods. Our results show a three-step hybrid H_2 storage pathway, *i.e.*, rapid enrichment, targeted capture, and dynamic transfer. Specifically, the ZIF-8 pores rapidly adsorb H_2 (via physisorption), increasing the local H_2 concentration (Fig. 7b). Subsequently, the hydrate crystal that grows under the promotion of THF, rapidly captures H_2 molecules (Fig. 7b). Finally, the adsorbed H_2 moves to the nucleating hydrate cages until the hydrogen source transfer reaches a dynamic equilibrium (Fig. 7b). Stronger physisorption increases the local H_2 concentration, allowing more H_2 molecules to be captured in the hydrate cages. These results exhibit a hybrid storage

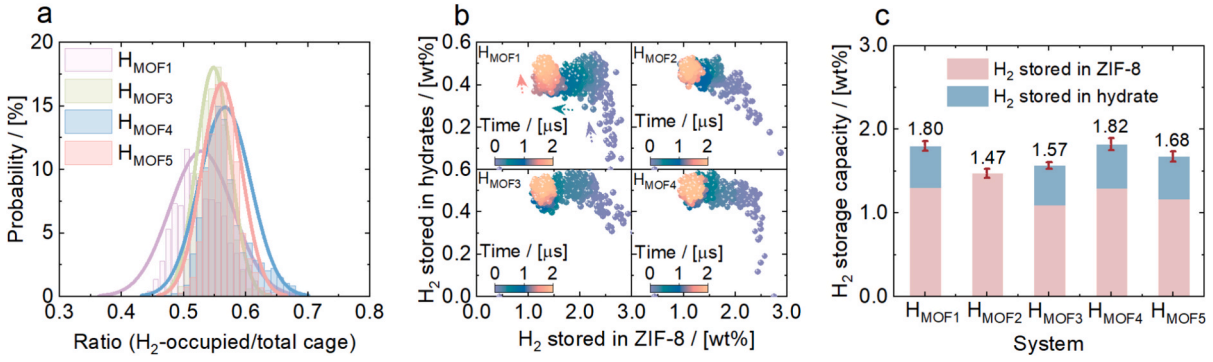

Fig. 7. (a) Probability distribution of the number ratio (H_2-occupied/total cages) and (b) H_2 stored in hydrates as a function of the H_2 stored in ZIF-8 for the four systems, *i.e.*, H_{MOF1}, H_{MOF3}, H_{MOF4}, and H_{MOF5}. (c) H_2 storage capacity via the hybrid H_2 physisorption-hydrate formation method averaged over the last 50 ns of the simulation.

mechanism for H_2 between ZIF-8 and hydrates. The hydrophobic ZIF-8 not only increases the local H_2 concentration but also provides an interface for water molecules to organize into cage-like structures, effectively combining physisorption and hydrate formation. As a result, the total H_2 storage capacity (physisorption and hydrate storage) in these systems over the last 0.05 μs of the 2 μs simulation far exceeds that achievable by a single mechanism, reaching 1.82 wt% (Fig. 7c). This also significantly exceeds the previously reported experimental storage capacity of 0.27 wt% for hydrate-based H_2 storage [22,23]. This system achieves a high H_2 storage capacity at 250 K and 50 MPa, indicating that efficient H_2 storage can be achieved solely through the synergistic effect of the THF promoter at pressures far below the 200 MPa required for pure H_2 hydrates. Compared to strategies relying solely on MOF adsorption or hydrates, this study shows that a hybrid approach combining ZIF-8 physisorption with THF-driven hydrate formation is a viable path for efficient H_2 storage. Notably, due to computational cost constraints, the simulation was stopped at 2 μs. As evidenced by Figs. S28b and S29a-e, the number of enclathrated H_2 molecules and the number of hydrate-bound water molecules exhibit a continuous upward trend without reaching a plateau. This persistent positive slope at the end of the trajectory indicates that the hydrate growth kinetics are still active and the system has not yet reached saturation, suggesting that the H_2 storage capacity would further increase over longer timescales. According to a previous study [11], the H_2 storage capacity of binary H_2-THF hydrate reached ca. 4 wt%. Assuming the complete conversion of the aqueous phase into an ideal hydrate structure, and accounting for the additional H_2 adsorbed in ZIF-8, the theoretical storage capacity of this hybrid system could potentially exceed 5 wt% given sufficient time. Molecular simulations of extended timescales would be a useful tool to showcase if these storage capacities can actually be reached. Our results show a three-step hybrid H_2 storage pathway, *i.e.*, rapid enrichment, targeted capture, and dynamic transfer. The ZIF-8 pores, acting as H_2 storage tanks, rapidly enrich H_2 through physisorption, increasing the local H_2 concentration. This H_2 tank is strategically positioned to continuously supply the hydrate growth front, thus, overcoming the fundamental limitation of low H_2 solubility in the aqueous phase. Subsequently, the growing binary H_2-THF hydrate crystals efficiently trap the enriched H_2 molecules that are readily available in the ZIF-8 pores. Finally, a continuous flux of H_2 will from the ZIF-8 pores to the encapsulating hydrate cages until the hydrogen source transfer reaches a dynamic equilibrium. From a practical perspective, the recovery of stored H_2 is achieved via the separation of the hydrate phase from the ZIF-8 framework following a controlled dissociation, rather than mechanical solid–solid separation. By applying thermal stimulation or depressurization, the hydrate lattice decomposes, leading to a spontaneous phase separation into H_2 gas, liquid water, and solid ZIF-8. This process allows for the effective extraction of H_2 while retaining the MOF structure. This dissociation-based separation pathway is conceptually similar to the post-treatment processes widely employed in hydrate-based desalination technologies, ensuring that the integration of ZIF-8 does not hinder the final recovery of the stored gas. However, the presence of the ZIF-8 host adds mass to the system. From a logistical perspective, the requirement to transport the entire solid composite implies that the ZIF-8 framework must be shipped to the point of use, and subsequently returned to the production facility for recycling. This cycle of transporting non-fuel mass increases operational costs and may limit the feasibility of this method for long-distance export. Therefore, this hybrid strategy is likely more advantageous for stationary storage applications where rapid charge/discharge kinetics are prioritized over transport efficiency. It should be noted that here a relatively high ratio of ZIF-8 to water is used to efficiently capture the nucleation events in timescales accessible to MD simulations. In practical engineering applications with lower solid concentrations, the diffusion of H_2 through the bulk aqueous phase may become a rate-limiting factor. To this purpose, our study serves as motivation for future studies investigating a broader range of ZIF-to-water ratios to quantitatively assess the impact of particle concentration on H_2 diffusion and the macroscopic kinetics of hydrate formation.

4. Conclusions

Microsecond-scale molecular dynamics simulations were performed to elucidate the hybrid H_2 physisorption-hydrate formation mechanism in the hydrophobic metal–organic framework ZIF-8 seeded with THF hydrate nanoparticles. To quantify the coupled effects of ZIF-8 physisorption and THF-driven hydrate growth on H_2 storage, five independent systems were studied at 250 K and 50 MPa. The simulation results indicate that ZIF-8 effectively prevents the permeation of H_2O and the larger THF promoter molecules into the pores, thereby establishing a gas–liquid interface between H_2 and the aqueous solution. Concurrently, ZIF-8 selectively captures and enriches H_2 molecules from the bulk phase through physisorption, reaching a high local H_2 concentration in its pores. This effectively transforms the MOF into a dedicated H_2 tank that is strategically positioned to continuously supply the hydrate growth front, thus, overcoming the fundamental limitation of low H_2 solubility in the aqueous phase. Our results strongly suggest that a dynamic, three-step hybrid H_2 storage mechanism takes place. (1) Rapid Enrichment, where the ZIF-8 pores act as nanoscopic storage tanks, rapidly concentrating H_2 via physisorption to increase the local H_2 concentration; (2) Targeted Capture, wherein the growing binary H_2-THF hydrate crystals efficiently trap the enriched H_2 molecules that are readily available in the ZIF-8 pores; (3) Dynamic Transfer, *i.e.*, characterized by a continuous flux of H_2 from the ZIF-8 pores to the encapsulating hydrate cages until the hydrogen source transfer reaches a dynamic equilibrium. Our simulations show that the hybrid system can achieve a total H_2 storage capacity of up to 1.82 wt% at a temperature of 250 K and a pressure of 50 MPa, exceeding the H_2 storage capacity of either physisorption or THF-driven hydrate formation alone. This work provides a foundational design principle for future H_2 storage materials, *i.e.*, rationally combining a hydrophobic, H_2-selective porous host with an effective hydrate promoter, it is possible to engineer a cooperative system that overcomes the kinetic and thermodynamic barriers of traditional storage methods. We also identified avenues for further improvement, such as reducing the number of empty cages and enhancing multi-occupancy rates, which point toward future research in optimizing MOF-promoter pairings and process conditions. These insights pave the way for the development of a new class of materials capable of achieving H_2 storage via a hybrid physisorption-hydrate formation method.

CRediT authorship contribution statement

Fengyi Mi: Writing – original draft, Visualization, Validation, Methodology, Investigation, Formal analysis, Conceptualization. **Hongjuan Sun:** Writing – review & editing, Formal analysis. **Wei Li:** Writing – review & editing, Data curation. **Bin Fang:** Writing – review & editing, Data curation. **Zhun Zhang:** Writing – review & editing. **Bowen Sha:** Validation, Data curation. **Thijs J.H. Vlugt:** . **Othonas A. Moultos:** Writing – review & editing, Data curation. **Fulong Ning:** Writing – review & editing, Resources, Funding acquisition, Data curation.

Declaration of competing interest

The authors declare that they have no known competing financial interests or personal relationships that could have appeared to influence the work reported in this paper.

Acknowledgements

This work was supported by the National Science Foundation for Distinguished Young Scholars (42225207), Natural Science Foundation of Hubei Province (2021CFA024), the National Natural Science

Foundation of China (42406219, 42206235), China Postdoctoral Science Foundation (2024 M76305), and China Scholarship Council (CSC202306410133). The authors acknowledge the use of computational resources of DelftBlue supercomputer, provided by Delft High Performance Computing Centre (https://www.tudelft.nl/dhpc).

Appendix A. Supplementary data

Supplementary data to this article can be found online at https://doi.org/10.1016/j.fuel.2026.138370.

Data availability

Data will be made available on request.

References

[1] Jena P. Materials for hydrogen storage: past, present, and future. J Phys Chem Lett 2011;2:206–11.
[2] Niaz S, Manzoor T, Pandith AH. Hydrogen storage: Materials, methods and perspectives. Renewable Sustainable Energy Rev 2015;50:457–69.
[3] Khan MI, Yasmin T, Shakoor A. Technical overview of compressed natural gas (CNG) as a transportation fuel. Renewable Sustain Energy Rev 2015;51:785–97.
[4] Zhang T, Uratani J, Huang Y, Xu L, Griffiths S, Ding Y. Hydrogen liquefaction and storage: Recent progress and perspectives. Renewable Sustainable Energy Rev 2023;176:113204.
[5] Cho ES, Ruminski AM, Aloni S, Liu Y-S, Guo J, Urban JJ. Graphene oxide/metal nanocrystal multilaminates as the atomic limit for safe and selective hydrogen storage. Nat Commun 2016;7:10804.
[6] Blankenship LS, Balahmar N, Mokaya R. Oxygen-rich microporous carbons with exceptional hydrogen storage capacity. Nat Commun 2017;8:1545.
[7] Sloan Jr ED. Fundamental principles and applications of natural gas hydrates. Nature 2003;426:353–9.
[8] Struzhkin VV, Militzer B, Mao WL, Mao HK, Hemley RJ. Hydrogen storage in molecular clathrates. Chem Rev 2007;107:4133–51.
[9] Mao WL, Mao HK, Goncharov AF, Struzhkin VV, Guo Q, Hu J, et al. Hydrogen clusters in clathrate hydrate. Science 2002;297:2247–9.
[10] Mao WL, Mao HK. Hydrogen storage in molecular compounds. Proc Nat Acad Sci USA 2004;101:708–10.
[11] Lee H, Lee JW, Kim DY, Park J, Seo YT, Zeng H, et al. Tuning clathrate hydrates for hydrogen storage. Nature 2005;434:743–6.
[12] Florusse LJ, Peters CJ, Schoonman J, Hester KC, Koh CA, Dec SF, et al. Stable low-pressure hydrogen clusters stored in a binary clathrate hydrate. Science 2004;306:469–71.
[13] Zhang Z, Kusalik PG, Guo G-J. Molecular insight into the growth of hydrogen and methane binary hydrates. J Phys Chem C 2018;122:7771–8.
[14] Zhang J, Li Y, Rao Y, Li Y, He T, Linga P, et al. Probing the pathway of H_2-THF and H_2-DIOX sII hydrates formation: Implication on hydrate-based H_2 storage. Appl Energy 2024;376:124289.
[15] Kanaujiya R, Metya AK, Choudhary N, Kumar R, Patra TK. Molecular dynamics insights into tetrahydrofuran-assisted formation of CH_4, CO_2, and H_2 gas hydrates. Phys Chem Chem Phys 2025;27:13991–9.
[16] Lee W, Kang DW, Ahn Y-H, Lee JW. Rapid formation of hydrogen-enriched hydrocarbon gas hydrates under static conditions. ACS Sustain Chem Eng 2021;9:8414–24.
[17] Zhang Y, Bhattacharjee G, Zheng J, Linga P. Hydrogen storage as clathrate hydrates in the presence of 1, 3-dioxolane as a dual-function promoter. Chem Eng J 2022;427:131771.
[18] Chen S, Wang Y, Lang X, Fan S, Li G. Rapid and high hydrogen storage in epoxycyclopentane hydrate at moderate pressure. Energy 2023;268:126638.
[19] Xie Y, Zhu Y-J, Cheng L-W, Zheng T, Zhong J-R, Xiao P, et al. The coexistence of multiple hydrates triggered by varied H_2 molecule occupancy during CO_2/H_2 hydrate dissociation. Energy 2023;262:125461.
[20] Zheng R, Mohammed S, Jia Y, Hazra R, Gadikota G. The effect of H_2 occupancy modes in small and large cages of H_2-tetrahydrofuran hydrates on the hydrates' stability and H_2 storage capacity. Phys Chem Chem Phys 2025;27:6532–45.
[21] Mi F, Ning F, Vlugt; TJH, Moultos OA. Molecular insight into hydrogen storage in clathrate hydrates: The effect of different promoters on the spontaneous nucleation of hydrogen hydrates studied via microsecond-scale molecular dynamics simulations. Chem Eng J 2025;512:162253.
[22] Zhang J, Li Y, Yin Z, Zheng XY, Linga P. How THF tunes the kinetics of H_2–THF hydrates? a kinetic study with morphology and calorimetric analysis. Ind Eng Chem Res 2023;62:21918–32.
[23] Zhang J, Li Y, Yin Z, Linga P, He T, Zheng XY. Coupling amino acid L-val with THF for superior hydrogen hydrate kinetics: implication for hydrate-based hydrogen storage. Chem Eng J 2023;467:143459.
[24] Bao W, Teng Y, Wang P, Li Y, Zhu J, Han S, et al. Molecular analysis of hydrogen-propane hydrate formation mechanism and its influencing factors for hydrogen storage. Int J Hydrogen Energy 2024;50:697–708.
[25] Wang P, Long H, Teng Y, Li Y, Li Y, Zhu J, et al. Investigation of hydrogen-propane hydrate formation mechanism and optimal pressure range via hydrate-based hydrogen storage. Fuel 2024;361:130791.
[26] Kong Y, Yu H, Liu M, Zhang G, Wang F. Ultra-rapid formation of mixed H_2/DIOX/THF hydrate under low driving force: Important insight for hydrate-based hydrogen storage. Appl Energy 2024;362:123029.
[27] Xu J, Yang X, Chen J, Meng Z, Wang X, Wang B, et al. Molecular study on the growth mechanism of CO_2-H_2 binary hydrate promoted by electric field. Fuel 2024;363:130924.
[28] Teng Y, Li Y, Huang T, Chen Y, Wang P, Wang B, et al. Hydrogen purification via hydrate-based methods: Insights into H_2-CO_2-CO hydrate structures, thermodynamics, and kinetics. Gas Sci Eng 2024;131:205484.
[29] Papadimitriou NI, Tsimpanogiannis IN, Papaioannou AT, Stubos AK. Evaluation of the hydrogen-storage capacity of pure H_2 and binary H_2-THF hydrates with monte carlo simulations. J Phys Chem C 2008;112:10294–302.
[30] Papadimitriou NI, Tsimpanogiannis IN, Economou IG, Stubos AK. Storage of H_2 in clathrate hydrates: Evaluation of different force-fields used in monte carlo simulations. Mol Phys 2017;115:1274–85.
[31] Tsimpanogiannis IN, Economou IG. Monte Carlo simulation studies of clathrate hydrates: A review. J Supercrit Fluids 2018;134:51–60.
[32] Nguyen NN, Nguyen AV. "Nanoreactors" for boosting gas hydrate formation toward energy storage applications. ACS Nano 2022;16:11504–15.
[33] Mi F, He Z, Pang J, Moultos OA, Vlugt; TJH, Ning F. Molecular insights into hybrid CH_4 Physisorption-hydrate formation in spiral halloysite nanotubes: implications for energy storage. ACS Appl Mater Interfaces 2024;16:67587–96.
[34] Farrando-Perez J, Balderas-Xicohtencatl R, Cheng Y, Daemen L, Cuadrado-Collados C, Martinez-Escandell M, et al. Rapid and efficient hydrogen clathrate hydrate formation in confined nanospace. Nat Commun 2022;13:5953.
[35] Ciocarlan RG, Farrando-Perez J, Arenas-Esteban D, Houlleberghs M, Daemen LL, Cheng Y, et al. Tuneable mesoporous silica material for hydrogen storage application via nano-confined clathrate hydrate construction. Nat Commun 2024;15:8697.
[36] Casco ME, Rey F, Jordá JL, Rudić S, Fauth F, Martinez-Escandell M, et al. Paving the way for methane hydrate formation on metal–organic frameworks (MOFs). Chem Sci 2016;7:3658–66.
[37] Denning S, Majid AA, Lucero JM, Crawford JM, Carreon MA, Koh CA. Metal-organic framework HKUST-1 promotes methane hydrate formation for improved gas storage capacity. ACS Appl Mater Interfaces 2020;12:53510–8.
[38] Duan J, Li Q, Fu Y, Chen S, Zhang Y, Liu D. Accelerated formation of hydrate in size-varied ZIF-8 for CH_4 storage by adsorption-hydration hybrid technology. Fuel 2022;322:124266.
[39] Zhang G, Liu Z, Kong Y, Wang F. Hydrate-based adsorption-hydration hybrid approach enhances methane storage in wet MIL-101(Cr)@AC under mild condition. Chem Eng J 2023;472:145068.
[40] Chen S, Duan J, Xie X, Fu Y, Zi M. Adsorption enhances CH_4 transport-driven hydrate formation in size-varied ZIF-8: Micro-mechanism for CH_4 storage by adsorption-hydration hybrid technology. Chem Eng J 2024;482:148957.
[41] Duan J, Jiang X, Fu Y, Chen S, Zi M. Molecular insights into CH_4/H_2O transport and hydrate formation in hydrophobic metal-organic frameworks ZIF-8: Implication for CH_4 storage by adsorption-hydration hybrid method. Fuel 2023;337:126851.
[42] Wang Z, Duan J, Chen S, Fu Y, Zhang Y, Wang D, et al. Molecular insights into hybrid CH_4 physisorption-hydrate growth in hydrophobic metal–organic framework ZIF-8: Implications for CH_4 storage. Chem Eng J 2022;430:132901.
[43] Chen L, Ting VP, Zhang Y, Coventry J, Rahbari A, Yin Z, et al. Hydrate-based H_2 storage with porous materials as heterogeneous promoters: state of the art and challenges. J Mater Chem A 2025.
[44] Suh MP, Park HJ, Prasad TK, Lim DW. Hydrogen storage in metal-organic frameworks. Chem Rev 2012;112:782–835.
[45] Sloan EDKC. Clathrate hydrates of natural gases. 3rd ed. Boca Raton, FL: CRC Press; 2008.
[46] Sheveleva A, Anikeenko A, Poryvaev A, Kuzmina D, Shundrina I, Kolokolov D, et al. Probing gas adsorption in metal–organic framework ZIF-8 by EPR of embedded nitroxides. J Phys Chem C 2017;121:19880–6.
[47] Zheng B, Sant M, Demontis P, Suffritti GB. Force field for molecular dynamics computations in flexible ZIF-8 framework. J Phys Chem C 2012;116:933–8.
[48] Jorgensen WL, Maxwell DS, TiradoRives J. Development and testing of the OPLS all-atom force field on conformational energetics and properties of organic liquids. J Am Chem Soc 1996;118:11225–36.
[49] Abascal JL, Sanz E, Garcia Fernandez R, Vega C. A potential model for the study of ices and amorphous water: TIP4P/Ice. J Chem Phys 2005;122:234511.
[50] Mi F, He Z, Ning F. Molecular dynamics simulation on CO_2 hydrate growth and CH_4-CO_2 replacement in various clay nanopores. Energy 2025;314:134282.
[51] Fengyi M, Zhongjin H, Guosheng J, Fulong N. Molecular insights into the effects of lignin on methane hydrate formation in clay nanopores. Energy 2023;276:127496.
[52] Mi F, He Z, Ning F. Molecular insight on CO_2/C_3H_8 mixed hydrate formation from the brine for sustainable hydrate-based desalination. Sep Purif Technol 2025;353:128244.
[53] Alavi S, Ripmeester JA, Klug DD. Molecular-dynamics study of structure II hydrogen clathrates. J Chem Phys 2005;123:24507.
[54] Wang Y, Yin K, Lang X, Fan S, Li G, Yu C, et al. Hydrogen storage in sH binary hydrate: insights from molecular dynamics simulation. Int J Hydrogen Energy 2021;46:15748–60.
[55] Hu W, Tian X, Chen C, Cheng C, Zhu S, Zhang J, et al. Molecular dynamic simulation of H_2-CH_4 binary hydrate growth induced by methane hydrate. Fuel 2024;360:130554.

[56] Kang DW, Lee W, Ahn Y-H, Lee JW. Exploring tuning phenomena of THF-H_2 hydrates via molecular dynamics simulations. J Mol Liq 2022;349:118490.
[57] Wang Y, Yin K, Fan S, Lang X, Yu C, Wang S, et al. The molecular insight into the "zeolite-ice" as hydrogen storage material. Energy 2021;217:119406.
[58] Mi F, He Z, Jiang G, Ning F. Effect of glucose on CH_4 hydrate formation in clay nanopores and bulk solution: Insights from Microsecond Molecular dynamics simulations. ACS Sustain Chem Eng 2024;12:4644–54.
[59] Rahbari A, Chakrapani TH, Shuang F, Krokidas P, Habibi P, Lagerweij VJ, et al. Molecular simulation of hydrogen systems: From properties and methods to applications and future directions. Chem Rev 2025.
[60] Mi F, Li W, Pang J, Moultos OA, Ning F, Vlugt; TJH. Molecular insights into the microscopic behavior of CO_2 hydrates in oceanic sediments: Implications for Carbon sequestration. J Phys Chem C 2024;128:18588–97.
[61] Mi F, Pang J, Li W, Moultos OA, Ning F, Vlugt; TJH. Novel pseudo-hexagonal montmorillonite model and microsecond MD simulations of hydrate formation in mixed clay sediments with surface defects. J Chem Phys 2024;161.
[62] Mi F, He Z, Jiang G, Ning F. What roles do interlayer cations (K^+) and salt ions (Na^+ and Cl^-) play in methane hydrate formation in illite nanopore? Appl Clay Sci 2024;256:107428.
[63] Nosé S. A Molecular-dynamics method for simulations in the canonical ensemble. Mol Phys 1984;52:255–68.
[64] Parrinello M, Rahman A. Crystal-structure and pair potentials - a molecular-dynamics study. Phys Rev Lett 1980;45:1196–9.
[65] Abraham MJ, Murtola T, Schulz R, Páll S, Smith JC, Hess B, et al. GROMACS: High performance molecular simulations through multi-level parallelism from laptops to supercomputers. SoftwareX 2015;1:19–25.
[66] Wang P, Li Y, Sun N, Han S, Wang X, Su Q, et al. Hydrate technologies for CO_2 capture and sequestration: status and perspectives. Chem Rev 2024;124:10363–85.
[67] Báez LA, Clancy P. Computer simulation of the crystal growth and dissolution of natural gas hydrates a. Ann NY Acad Sci 1994;715:177–86.
[68] Alavi S, Ripmeester JA. Simulations of hydrogen gas in clathrate hydrates. Mol Simul 2017;43:808–20.